A Synthetic Probiotic Engineered for Colorectal Cancer Therapy Modulates Gut Microbiota

Yusook Chung
Cell Biotech, Co., Ltd.
Yongku Ryu
Cell Biotech, Co., Ltd.
Byung Chull An
Cell Biotech, Co., Ltd.
Yeo-Sang Yoon
Cell Biotech, Co., Ltd.
Oksik Choi
Cell Biotech, Co., Ltd.
Tai Yeub Kim
Cell Biotech, Co., Ltd.
Jae Kyung Yoon
Yonsei University
Jun Young Ahn
Cell Biotech, Co., Ltd.
Ho Jin Park
Cell Biotech, Co., Ltd.
Soon-Kyeong Kwon
Yonsei University
Jihyun F. Kim (jfk1@yonsei.ac.kr)
Yonsei University https://orcid.org/0000-0001-7715-6992
Myung Jun Chung (ceo@cellbiotech.com)
Cell Biotech, Co., Ltd.

Research

Keywords: Lactobacillus rhamnosus CBT LR5 (KCTC 12202BP), alanine racemase, DLD-1 xenograft, AOM/DSS model of colitis-associated cancer, microbiome, Akkermansia, Turicibacter

Posted Date: August 13th, 2020

DOI: https://doi.org/10.21203/rs.3.rs-56674/v1

Abstract

Background: Successful chemoprevention or chemotherapy is achieved through targeted delivery of prophylactic agents during initial phases of carcinogenesis or therapeutic agents to malignant tumors. Bacteria can be used as anticancer agents, but efforts to utilize attenuated pathogenic bacteria suffer from the risk of toxicity or infection. Lactic acid bacteria are safe to eat and often confer health benefits, making them ideal candidates for live vehicles engineered to deliver anticancer drugs.

Results: In this study, we developed an effective bacterial drug delivery system for colorectal cancer (CRC) therapy using the lactic acid bacterium *Pediococcus pentosaceus*. It is equipped with dual gene cassettes driven by a strong inducible promoter that encode the therapeutic protein P8 fused to a secretion signal peptide and a complementation system. In an inducible CRC cell-derived xenograft mouse model, our synthetic probiotic significantly reduced tumor volume and inhibited tumor growth relative to the control. Mice with colitis-associated CRC induced by azoxymethane and dextran sodium sulfate exhibited polyp regression and recovered taxonomic diversity when the engineered bacterium was orally administered. Further, the synthetic probiotic modulated gut microbiota and alleviated the chemically induced dysbiosis. Correlation analysis demonstrated that specific bacterial taxa potentially associated with eubiosis or dysbiosis, such as *Akkermansia* or *Turicibacter*, have positive or negative relationships with other microbial members.

Conclusions: Taken together, our work illustrates that an effective and stable synthetic probiotic composed of *P. pentosaceus* and the P8 therapeutic protein can reduce CRC and contribute to rebiosis, and the validity and feasibility of cell-based designer biopharmaceuticals for both treating CRC and ameliorating impaired microbiota.

Background

Cancer is the leading cause of death in humans and the global burden is rising [1]. Cancer treatments include surgery, chemotherapy, radiotherapy, and targeted therapy. In chemotherapy, natural, synthetic, or biological substances are used as treatments that suppress or prevent cancer progression [2]. However, most chemotherapeutic agents target rapidly dividing cells, which not only include cancer, but bone marrow or hair follicles as off-target effects. Moreover, drug resistance diminishes the efficacy of chemotherapy and is responsible for the high relapse rate even after successful recovery. Targeted therapy commonly uses biopharmaceuticals that are more specific, less toxic, and rarely cause side effects; however, the selectivity is often insufficient in practice [3, 4].

Bacteria can be utilized to treat cancer and their recognition as anticancer agents dates back more than a century [5]. Strains of potentially harmful or pathogenic bacteria like *Clostridium*, *Listeria*, or *Salmonella* that are either natural, mutated, or genetically modified have been used in cancer therapy due to their ability to colonize the solid tumor under hypoxic conditions and induce tumor shrinkage [6]. Although there have been efforts to make use of attenuated bacteria, the risk for toxicity or infection hampers their

clinical applications. Generally recognized as safe and often with health benefits for the host, lactic acid bacteria (LABs) such as *Lactobacillus*, *Lactococcus*, *Leuconostoc*, or *Pediococcus*, are ideal candidates for bacterial therapy [7, 8]. Furthermore, they can be used as live vehicles engineered to deliver anticancer drugs [9].

CRC is a severe cancer responsible for almost 900,000 deaths annually [10]. A small protein called P8 with a molecular mass of 8 kDa was isolated from *Lactobacillus rhamnosus* CBT LR5, in an effort to screen for novel therapeutic proteins against CRC [11]. To design and develop a clinically relevant system that can be orally administered and still stable, we used an LAB strain, *Pediococcus pentosaceus* SL4 [12], as a safe drug delivery vehicle that expresses and secretes P8 and thus, avoid its degradation in the gastrointestinal tract. We isolated the *P. pentosaceus* SL4 bacterium from a Korean fermented vegetable food, kimchi, which produces a bacteriocin and inhibits the growth of *Listeria monocytogenes* and *Staphylococcus aureus* [13]. *P. pentosaceus* is Gram-positive, facultatively anaerobic, acid-tolerant, non-motile, and non-spore-forming [12]. It is frequently isolated from fermented foods and applied as the starter culture in dairy or plant fermentation [14, 15]. Strains of this species were able to alleviate azoxymethane-induced toxicity, inhibit colon cancer cell proliferation, and secrete antimicrobial peptides that inhibit pathogenic bacteria [16–18].

In this study, we developed an advanced anti-CRC therapeutic probiotic that utilizes P8 and demonstrated its powerful efficacy using two different murine models: DLD-1 xenograft and colitis-associated tumorigenesis induced by azoxymethane (AOM) and dextran sodium sulfate (DSS). Moreover, considering the significant relationship between gut microbiota and drug response [19], we longitudinally investigated microbiota profiles during the administration of the P8-producing synthetic probiotic in the AOM/DSS model to reveal the complex interactions between individual microbial members and to identify key taxa associated with use of our synthetic probiotic and AOM/DSS-induced tumorigenesis.

Results

Designing an effective drug delivery system for CRC therapy

Fig. 1a depicts the design principle of a synthetic probiotic that employs the P8 therapeutic protein to treat or prevent CRC. To design an anti-CRC therapeutic probiotic with enhanced stability and efficacy, we first adopted the *alr* complementation system that can prevent curing of the P8 expression vector, pCBT24-2 [11], in the absence of an antibiotic to maintain the plasmid. Alanine racemase is a pyridoxal 5′-phosphate-dependent enzyme involved in the interconversion of d-alanine (d-Ala) and l-alanine. d-Ala is involved in the cross-linking of the cell wall peptidoglycan layer and exists in extremely low amounts in nature. Thus, this component is essential for bacterial growth and deletion of the *alr* gene leads to cell death. To generate a d-Ala auxotroph of *P. pentosaceus* SL4(-7) that is a derivative of SL4 lacking all seven native plasmids, we performed knockout mutagenesis to remove *alr* from the chromosome using homolog recombination with a construct that has an in-frame deletion of the *alr* gene and 1 kb of its upstream or downstream flanking sequences (Additional file 1, Fig. S1a,b). The resulting auxotrophic

mutant was either grown in a medium supplemented with d-Ala or complemented with a plasmid that expresses *alr*. Genotyping with specific primers confirmed the replacement of the intact gene (Additional file 1, Fig. S1c, Additional file 2, Table S1). This *alr* auxotroph complemented with plasmid-borne *alr* was designated as PP*.

In order to develop an effective gene expression system that can maximize the productivity of P8, four kinds of constitutive promoters involved in central glycolytic pathway: pyruvate kinase (PK), choline ABC transporter permease and substrate binding protein, glucose kinase, and l-lactate dehydrogenase. Using these promoters, we constructed five sets of dual expression systems that have two chimeric genes, each encoding the P8 peptide fused to the Usp45 secretion signal at its N terminus, which was cloned into the vector that contained *alr* (Fig. 1b). We then measured the concentrations of secreted P8 for each PP* clone with the dual expression module in the *alr* vector using ELISA to validate the PK-PK promotor system with the best stability and productivity (Fig. 1c). To further exclude the possibility that the host genotype could affect the performance of P8 secretion, we checked the concentrations of P8 secreted from the wild type *P. pentosaceus* SL4(-7) with the PK-PK promotor system in pCBT24-2 (PP-P8) and the *Δalr* mutant with the PK-PK promotor system in the *alr* vector (PP*-P8) and found no difference between the SL4 wild type and *Δalr* mutant (Additional file 1, Fig. S1d).

Anti-tumor efficacy of PP*-P8 in the DLD-1 xenograft mouse model

To determine whether PP*-P8 had anticancer activity *in vivo*, we assessed its efficacy using the DLD-1 xenograft mouse model. Athymic BALB/c nude mice with subcutaneous DLD-1 xenografts were treated with the commercial chemotherapy drug gemcitabine, PP* or PP*-P8 (see Materials and Methods for dose and dosage regimen), and the tumor sizes were monitored for 6 weeks before sacrifice (Fig. 2, Additional file 2, Supplementary Tables 2 and 3). Tumor growth rate was much faster in the untreated control group and the PP*-treated group than in those treated with gemcitabine or PP*-P8 (Fig. 2a). At the end of the experiment, the mean tumor volumes were 2,680.9±419.7 mm^3 in the control group and 2,671.1±651.2 mm^3 in the PP* group, while they were 498.6±192.7 mm^3 and 1,371±349.8 mm^3 in the gemcitabine and PP*-P8 treatment groups, respectively (Fig. 2a,b; control vs. PP*-P8, $P = 4.9\times10^{-5}$). Tumor weights were 2.13±0.31 g in the control and 2.35±0.32 mm^3 in PP*, as compared to 0.39±0.16 g in gemcitabine and 0.97±0.30 g in PP*-P8 (Additional file 1, Fig. S2a; control vs. PP*-P8, $P < 1\times10^{-6}$). Inhibition ratios of tumor growth relative to the control were 84.1% and 50.8% in gemcitabine and PP*-P8, respectively (Fig. 2c; control vs. PP*-P8, $P = 5.3\times10^{-5}$). These results demonstrate that our synthetic probiotic PP*-P8 sufficiently suppressed tumor growth similar to that of an anticancer drug.

Next, we asked whether the growth inhibition of the CRC xenograft induced by PP*-P8 is due to cell cycle arrest. Western blot analysis revealed that expression of cell cycle regulatory factors Cyclin B1 and Cdk1 in tumor tissue decreased significantly in response to treatment with PP*-P8 (Fig. 2d, Additional file 1, Fig. S2b). Moreover, expression of p21, which suppresses Cyclin B1/Cdk1, increased after PP*-P8 treatment. In addition, expression of p53 also increased in the PP*-P8-treated group. Overall, the data suggest that

the anticancer therapeutic protein P8 inhibits the p53-p21 signaling pathway, resulting in G2 arrest of DLD-1 cells.

PP*-P8 attenuates tumorigenesis associated with AOM/DSS-induced colitis

We also used the well-established AOM/DSS-inducible murine model for colitis-associated colon carcinogenesis to examine the anticancer effect of the synthetic probiotic PP*-P8 *in situ*. During the whole experimental period of 68 days, AOM was intraperitoneally injected into C57BL/6 mice on day 1, followed by three treatments of DSS administered in the animal drinking water. The mice were divided into five groups: untreated control (AOM/DSS only), gemcitabine, wild type *P. pentosaceus* SL4 (PP WT), PP*, and PP*-P8 (Fig. 3a; see Materials and Methods for dose and dosage regimen). Analysis of the relative abundance of the *Pediococcus* bacteria in the three groups indicated that bacterial populations were sustained at 0.01~0.03% (Fig. 3b; see Materials and Methods for microbial community analysis). Although the population of *Pediococcus* in PP WT increased during stage 1 as compared to PP* and PP*-P8, the three groups showed similar relative abundances in the subsequent two stages until the end of the experiment.

Drastic changes in the average bleeding score were observed before and after each episode of DSS administration (Fig. 3c; $P = 3.12\times10^{-2}$ between day 5 and 10, $P = 6.40\times10^{-7}$ between day 26 and 31, and $P = 1.90\times10^{-6}$ between day 47 and 52). The gemcitabine and PP*-P8 groups showed significantly reduced bleeding after the administration of DSS compared to the untreated ($P = 8\times10^{-6}$), PP WT ($P = 8.68\times10^{-2}$) and PP* ($P = 2.42\times10^{-4}$) control groups (Additional file 2, Supplementary Tables 4 and 5). Severe bleeding and bleeding around the anus were often noticeable in the controls, whereas only occult blood or slight bleeding was detected for PP*-P8. Fig. 4a as well as Supplementary Tables 4 and 5 in Additional file 2 show that DSS treatment had negative effects on weight gain in the gemcitabine and control groups, while body weight of mice in the PP*-P8 group increased until the end of the experiment. Kaplan–Meier survival curves similarly showed that, with no fatalities, PP*-P8 treatment increased the survival of AOM/DSS-treated mice during the experiment, although this increase was not statistically significant compared to the control groups (Additional file 1, Fig. S3). Colon length is one of the markers for evaluating colonic inflammation severity, and was measured after animals were euthanized to reveal that gemcitabine and the three controls had significantly decreased colon lengths in comparison to PP*-P8 ($P < 1\times10^{-6}$, $P < 1\times10^{-6}$, $P = 1\times10^{-6}$ for untreated, PP WT, PP*, respectively), which was indicative of severe inflammation (Fig. 4b). In comparison to the colon length of untreated control, which was administered with AOM/DSS only, the colon length of PP*-P8 exhibited close to that of the healthy mouse group, indicating that PP*-P8 treatment prevents the colon from being shortened due to the presence of AOM/DSS (Additional file 1, Table S4).

The number of nodular polypoid tumors located in the middle and distal colon in the PP*-P8 treatment group was lower than those in untreated control ($P = 2.32\times10^{-3}$) and PP* ($P = 1.24\times10^{-3}$) groups, while there was no significant change in PP WT ($P = 0.27$) (Fig. 4c,d). Taken together, these results from the

AOM/DSS-induced colitis-associated cancer model indicate that the orally administered PP*-P8 probiotic effectively inhibited inflammation-associated carcinogenesis and tumor development in the colon.

PP*-P8 modulates gut microbiota to alleviate AOM/DSS-induced dysbiosis

We further explored the possible impacts of the synthetic probiotic PP*-P8 on gut microbiota in the AOM/DSS murine model for colitis-associated colon cancer. C57BL/6 mice were subjected to a dose regimen and a fecal sampling schedule that was divided into untreated control, fluorouracil, PP WT, PP*, and PP*-P8 treatment groups (Fig. 3a). Using DNA from the fecal samples, amplicon sequencing of the V3–V4 region of the 16S ribosomal RNA gene was performed to monitor microbial community structure. Processed reads were clustered into operational taxonomical units (OTUs) with a 97% threshold for sequence identity using QIIME [20] to calculate relative abundance (Additional file 2, Supplementary Tables 6 and 7).

Species richness and evenness were measured by the number of OTUs and the inverse Simpson index, respectively, to evaluate microbial diversity, which was severely disturbed by AOM/DSS treatment (Fig. 5a). As expected, all the experimental groups lost alpha diversity, which reduced the number of OTUs during each DSS administration; however, the OTUs partially recovered until the next administration. Interestingly, the PP*-P8 group seemed to restore taxonomic diversity in stage 3 better than the fluorouracil and control groups toward the end of the experiment (red lines in Fig. 5a). Principal coordinates analysis (PCoA) based on Bray-Curtis dissimilarity [21] illustrated the dissimilarities of fecal microbiota between each treatment group and pre-treated samples on day 0 and day 5 increased as stages of treatment progressed (Additional file 1, Fig. S4). The differences between the controls, fluorouracil, and PP*-P8 treatments were not obvious during stage 1 (Fig. 5b, Additional file 1, Fig. S4); however, beta diversity increased over time and permutational multivariate analysis of microbial variance resulted in significant statistical differences among the groups in stages 2 and 3 ($P = 0.034$ and $P = 0.001$, respectively). The PCoA plots also show that the three control groups became more dispersed in stages 2 and 3 than PP*-P8. It is noteworthy that fluorouracil and PP*-P8 appeared similar in stage 3 (bottom panel of Fig. 5b).

Distribution and abundance of microbial taxa for each group in each stage were examined and the results indicated that bacteria in the *Bacteroidetes* and *Firmicutes* phyla dominated the mouse gut microbiota (Additional file 2, Table S7). Relative abundance at the family level illustrated that on day 0 *Muribaculaceae*, *Lachnospiraceae*, *Ruminococcaceae*, and *Lactobacillaceae* were the main families, while during DSS administration *Akkermansiaceae*, *Bacteroidaceae*, and *Erysipelotrichaceae*, as well as *Muribaculaceae*, *Lachnospiraceae*, *Lactobacillaceae*, and *Ruminococcaceae* were the primary bacteria (Fig. 5c). The relative abundance of each family fluctuated and depended on the stage of the DSS treatment. When compared to the control, the most distinguishable beta diversity pattern was observed at stage 3 (Fig. 5b; $P = 0.001$), and the fluorouracil-treated group was enriched with *Akkermansiaceae*, *Lachnospiraceae*, and *Ruminococcaceae*, but depleted of *Erysipelotrichaceae* and *Lactobacillaceae*. In the PP*-P8 treatment group, *Akkermansiaceae*, *Lachnospiraceae*, and *Lactobacillaceae* increased, while

Erysipelotrichaceae decreased compared to the controls. Our data from the AOM/DSS mouse model demonstrate that the PP*-P8 probiotic contributes to alleviating dysbiosis induced by AOM/DSS by modulating gut microbiota structure with respect to alpha and beta diversity, and the proportion of potentially beneficial taxa.

Specific bacterial taxa are associated with eubiosis maintained by PP*-P8

To determine which bacteria are most likely responsible for the differences between the treatment groups, we applied the linear discriminant analysis (LDA) and effect size (LEfSe) [22] method to calculate the LDA scores for days 56, 63, and 68 in stage 3 when the mice are recovering from the last DSS administration. The lists of taxonomic clades, ranked according to the effect size, that are differential among groups with statistical and biological significance are shown in Fig. 6a. They indicated that, between the fluorouracil and control groups, most discriminative ($\log_{10}$ LDA $\geq$ 4.0) in fluorouracil included *Actinobacteria* (phylum), *Coriobacteriales*, *Bifidobacteriales*, *Actinobacteria* (class), *Bifidobacteriaceae*, *Bifidobacterium*, and *Coriobacteriaceae* UCG_002, while one in the control was *Turicibacter*. Between PP*-P8 and the control, an uncultured *Ruminococcaceae* (OTU 330333), *Akkermansia*, *Verrucomicrobiae*, *Verrucomicrobia*, *Verrucomicrobiales*, *Akkermansiaceae*, GCA_900066575 (*Lachnospiraceae*), *Oscillibacter*, *Pediococcus*, *Tannerellaceae*, and *Parabacteroides* were most discriminative in PP*-P8, whereas *Turicibacter*, *Erysipelotrichia*, *Erysipelotrichaceae*, *Erysipelotrichales*, and *Firmicutes* were in the control. Similarly, *Akkermansia*, *Verrucomicrobiae*, *Akkermansiaceae*, *Verrucomicrobia*, *Verrucomicrobiales*, *Oscillibacter*, and an uncultured *Ruminococcaceae* (OTU 330333) were most differential in PP*-P8, whereas an uncultured *Muribaculaceae* (OTU 182112), *Muribaculaceae*, *Bacteroidetes*, *Turicibacter*, *Erysipelotrichia*, *Erysipelotrichaceae*, *Erysipelotrichales*, *Bacteroidales*, *Bacteroidia*, an unassigned *Rhodospirillales*, *Dubosiella*, and *Catenibacterium* were in PP*. Between PP*-P8 and fluorouracil, *Bacilli* at various taxonomic ranks down to *Lactobacillus*, *Tannerellaceae*, and *Parabacteroides* were most distinctive in PP*-P8, and an uncultured *Muribaculaceae* (OTU 182112), *Muribaculaceae*, and *Actinobacteria* at various ranks down to *Bifidobacterium* were in fluorouracil (Additional file 1, Fig. S5). LEfSe plots of OTUs between the groups at stage 3 showed a similar tendency (Additional file 1, Fig. S6) in that *Akkermansia* was the most discriminative genus in PP*-P8 ($\log_{10}$ LDA = 4.72), while *Turicibacter* was for the control ($\log_{10}$ LDA = 4.99).

Overall, the LEfSe results after the last DSS administration showed that *Akkermansia* and *Verrucomicrobia* at various ranks, to which *Akkermansia* belongs, followed by an uncultured *Ruminococcaceae* (OTU 330333) and *Oscillibacter*, were most characteristic of PP*-P8, and *Turicibacter* and *Erysipelotrichia* at various ranks, to which *Turicibacter* belongs, were characteristic of the control (Fig. 6b). *Akkermansia* was higher in PP*-P8 and fluorouracil than in the controls, and the uncultured *Ruminococcaceae* and *Oscillibacter* were abundant in PP*-P8 and PP WT. *Turicibacter* was highly enriched in the control and dramatically reduced in the other treatment groups, which was most noticeable in the PP*-P8 and fluorouracil groups. To identify the interactions between members of gut microbiota, a pairwise Spearman's rank correlation coefficient was calculated for the last three samples

on days 56, 63, and 68 in stage 3 and visualized as a heat map for systematic analysis (Fig. 6c). *Akkermansia*, the signature taxon of the PP*-P8 group's microbial profile, had a highly negative correlation with *Turicibacter*, which is a biomarker for control, and an uncultured member of *Muribaculaceae* (OTU 1107458). Also, two members of *Muribaculaceae* (OTU 270451, OTU 259609) had strong negative correlations with a member of *Lactobacillus* (OTU 463794) and two members of *Bacteroides* (OTU 4226929, OTU 513445). Another member of *Muribaculaceae* (OTU 322372) had a similar relationship with *Lactobacillus* and *Bacteroides*. These results suggest that specific bacterial taxa such as *Akkermansia* and *Turicibacter* are associated with eubiosis or dysbiosis, respectively, and positive or negative relationships among microbial members shape the community structure.

Discussion

Advances in the mechanistic understanding as well as diagnosis and treatment of cancer has increased the success rate of recovery, but there remain concerns about the side effects and drug resistance associated with current treatment programs. Among biopharmaceutical approaches to cancer treatment, efforts to apply live bacteria as therapy were verified in preclinical or early clinical trials; although they still have toxicity issues, these are genetically attenuated to less virulent or toxin-free levels [23–25].

Similar to that reported in our work, commensal bacteria recently received substantial attention from their potential for suppressing or preventing CRC [26–29]. Previously, we discovered a novel therapeutic peptide originating from a probiotic LAB strain and confirmed its clinical potential for the anti-CRC efficacy using a recombinant form [11]. In the present study, we established a stable and efficient DDS by adopting a d-Ala auxotrophic mutant of the food-grade LAB *P. pentosaceus* SL4(-7) complemented with an *alr*-containing plasmid expressing dual gene cassettes under the control of the PK-PK promotor system. Each of these cassettes encode a signal peptide for secretion that can be fused with a therapeutic protein. We then loaded the bacterium with the novel therapeutic protein P8 from *L. rhamnosus* CBT LR5 that has a strong anti-proliferative activity against DLD-1 cells [11, 30], to engineer the PP*-P8 synthetic probiotic for CRC therapy. Its efficacy was validated by two different murine models, DLD-1 xenograft and AOM/DSS-induced CRC. The xenograft model showed that our synthetic probiotic effectively inhibits the growth of tumors and can be a competitive therapeutic strain. The AOM/DSS model was used to longitudinally evaluate the inhibitory effects of our synthetic probiotic on carcinogenesis and demonstrated normal body weight and colon length, as well as a reduced bleeding score, fatality, and number of polyps, in the PP*-P8-treated mice as compared to controls.

There is an increasing awareness of the roles of the gut microbiome in influencing the response to and outcome of chemotherapy [19, 31, 32]. Reciprocal modification of the microbiota by chemotherapeutic agents is also increasingly appreciated. One important observation from our AOM/DSS experiment is that the PP*-P8 probiotic modulates the gut microbiota structure to alleviate the change from eubiosis to dysbiosis induced by AOM/DSS. Loss of diversity, increase deleterious and hallmarks of the unhealthy status of microbiota in the gut [33]. Recovery of alpha diversity and coherence of the microbial communities after three DSS treatments were most prominent in the PP*-P8 group, suggesting that our

synthetic probiotic is not only effective in treating CRC but also helpful in maintaining the microbiota structure and possibly securing host health benefits. Increased body weight and colon length measured in PP*-P8-treated mice support this hypothesis [34]. Apart from the anticancer effect, the rapid weight loss and the shortening of colon length in the gemcitabine-treated group were consistent with previously studied cases and are indicative of the double-sidedness of chemotherapy [35–37].

Results from LEfSe between groups enlisted specific microbial taxa that are discriminative with statistical and biological significance during PP*-P8 treatment in the AOM/DSS model. Among the taxa identified, most notable was the *Akkermansia-Verrucomicrobia* clade. *Akkermansia muciniphila* is a well-known biomarker for defining the healthy gut microbiota and thus, is considered a promising candidate for next-generation probiotics [38–40]. Conversely, *Turicibacter* was most characteristic of the untreated control. Type strain of *Turicibacter sanguinis* was isolated from the blood culture of a febrile patient with acute appendicitis [41]; moreover, some *Turicibacter* bacteria are reported to have a pathobiont lifestyle [42] and are often relevant to host inflammation [43–45]. Similarly, *Akkermansia* and *Turicibacter* had a significantly negative correlation to each other based on Spearman's correlation coefficient. We therefore hypothesize that the PP*-P8 probiotic coordinates the microbial consortium to maintain eubiosis during AOM/DSS-induced colitis-associated carcinogenesis, and likely helps improve drug response and reduce relapse rate.

It is interesting that the microbial communities of mice treated with PP*-P8 or fluorouracil [46] were similar at stage 3 in the AOM/DSS model, and both treatment groups presented high *Akkermansia* and low *Turicibacter* populations. With the exception of their effects on cancer development inhibition, it is unclear how these two treatments fundamentally different in nature affect the microbiota structure to resemble each other. It seems though that they influence the microbiota through different mechanisms of action, either directly or indirectly. Indeed, other than *Akkermansia*, lactobacilli and *Parabacteroides*, as well as the treated *Pediococcus*, were distinctive in PP*-P8, while an uncultured *Muribaculaceae* and bifidobacteria were in fluorouracil. It should be cautioned, however, to conclude that fluorouracil administration during AOM/DSS treatment has health benefits because the molecule itself causes various side effects that include DNA damage and inflammation [46–50].

Conclusions

Our approach to treating CRC with a stable and effective synthetic probiotic presents the validity and feasibility of cell-based designer biopharmaceutical agents. Our results also bear testimony to the positive or negative influences of biopharmaceuticals as well as chemotherapeutics on gut microbiota and possibly general health. Considering their potential impact, we suggest scrutinizing the dynamics of the microbiome and associated health issues during development of pharmaceuticals that are targeted to treat or prevent cancer, including CRC.

Methods

Bacterial strains and culture

The anticancer protein P8 was identified from *Lactobacillus rhamnosus* CBT LR5 (= KCTC 12202BP) isolated from the human intestine. *P. pentosaceus* SL4(-7) is a derivative of *P. pentosaceus* SL4 (= KCTC 10297BP) that was used as a drug delivery vehicle and isolated from the traditional Korean fermented vegetable kimchi. These strains were derived from the culture collection of Cell Biotech Co., Ltd., Gimpo, Korea, and routinely statically cultured at 37 ℃ for 18–24 h in Man, Rogosa and Sharpe (MRS) broth (Difco, Detroit, MI, USA) or M9 broth with 1% glucose for protein expression. *Escherichia coli* strain DH5α was cultured for 18–24 h in Luria-Bertani (LB) broth (Difco) at 37 ℃.

Cell culture

The human CRC cell line DLD-1 was purchased from the Korean Cell Line Bank and maintained under 5% CO_2 and 37 ℃ in Roswell Park Memorial Institute (RPMI)-1640 medium (Gibco, Grand Island, NY, USA) containing 10% fetal bovine serum (Gibco) and 1% penicillin/streptomycin (Gibco).

Construction of a plasmid-encoded *alr* complementation system

We followed the genetic design of the d-Ala auxotrophic PP as previously described [51]. To generate DNA fragments flanking the *alr* gene, we synthesized the regions Hr1 and Hr2 1-kb upstream and downstream of *alr* and the Amp-resistant gene in between Hr1-Amp^R-Hr2, and then cloned it into pCBT24-2 (KCCM12182P). The in-frame deletion of *alr* was made by homolog-recombination with a pCBT24-2-alrHr1,2-Amp^R construct. After electroporation (1.24 kV, 25 μF, 1 mm cuvette), among of PP transformants, the d-Ala auxotrophic PP was selected using MRS agar with 10 μg/ml erythromycin. The in-frame deletion mutants (*Δalr*) were screened on MRS agar containing erythromycin and 200 μg/ml d-Ala, and then the selected mutant was verified by PCR using the primers shown in Table S1 in Additional file 1,. The PCR product was sequenced and verified. Selected mutants were complemented with the pCBT24-2-alr plasmid for the *alr* auxotroph complementation system *P. pentosaceus alr* (pCBT24-2-alr), PP*.

Construction of the P8 dual-promoter gene expression systems

Two-promoter systems were introduced for maximal production of P8 in PP*. Usp45-P8 fragments were fused with five pairs of two promoter sets (Cosmo Genetech Co., Ltd., Seoul, Korea), PK-Usp45-p8-PK-Usp45-p8, PK-Usp45-P8-ChoS-Usp45-p8, GK-Usp45-p8-PK-Usp45-p8, GK-Usp45-p8-GK-Usp45-p8, and GK-Usp45-p8-LDH-Usp45-p8. Each expression system was inserted into the pCBT24-2-alr plasmid using *Nhe*I/*Sal*I and *BamH*I/*Pst*I restriction enzymes and transformed into the *alr* knockout mutant. Finally, the pCBT24-2-PK-p8-PK-p8-alr plasmid (accession number: KCCM12181P) was selected as DDS for P8 (Additional file 1, Fig. S1a).

ELISA analysis of P8 concentration

A 96-well polystyrene plate (SPL life sciences; Pocheon-si, Gyeonggi-do, Korea) was coated with 100 µl diluted anti-P8 IgG (1:5500 poly clonal-rabbit; Young In Frontier Co., Ltd., Seoul, Korea) in ELISA coating buffer (Bethyl Laboratories; Montgomery, TX, USA) overnight at 4°C. After coating, the wells were washed twice with 300 µl wash buffer (1× Tris-Buffered-Saline Buffer (TBS) with 0.05% Tween 20 (TBS-T)) followed by blocking with 300 µl blocking buffer (1× phosphate-buffered saline (PBS) and 5% fetal bovine serum (FBS; Gibco)) for 1 h at room temperature (RT). The wells were washed three times with 300 µl wash buffer prior to adding 100 µl protein samples (culture supernatant or mouse serum), followed by a 150 min incubation at RT. After sample binding, the wells were washed four times with 300 µl wash buffer (TBS-T) followed by primary antibody binding with 100 µl biotinylated anti-P8 IgG (500 pg/ml anti-P8 IgG-biotin; Young In Frontier Co., Ltd.) in 1× PBS with 5% FBS followed by a 90 min incubation at RT. After primary antibody binding, the wells were washed four times with 300 µl wash buffer (TBS-T), followed by secondary antibody binding with 100 µl streptavidin-HRP (166 pg/ml Young In Frontier Co., Ltd.) in 1× PBS with 2.5% FBS and incubated for 30 min at RT. After secondary antibody binding, the wells were washed four times with 300 µl wash buffer (TBS-T) followed by color development with 100 µl TMB one solution (Bethyl Laboratories) for 20 min at RT under dark and then 50 µl stop buffer (Bethyl Laboratories). Absorbance was measured using the multifunctional microplate reader (SpectraMax M5; Molecular Devices, Sunnyvale, CA, USA). A standard curve for the recombinant P8 sera dilution (2-fold dilutions 1000 pg/ml to 15.625 pg/ml) was performed in triplicate. Each sample was assayed in two different dilutions and run in duplicate. Results are reported in picogram amounts per milliliter PP*-P8 protein.

Mouse strains and growth conditions

Male athymic nude mice (BALB/cAnN.Cg-Foxn1nu/CrlNarl; five weeks of age, 50 in total for the CRC xenograft model) and male C57bL-6J mice (C57bL-6J; eight weeks of age, 50 in total for AOM/DSS induced CRC model) were purchased from SR Bio (Gyeonggi-Do, Korea). Mice were housed at constant temperature (20±3 ℃) and humidity (40±20%) with a 12/12-h light/dark cycle in a specific pathogen-free facility (Laboratory Animal Center of Cell Biotech Co., Ltd., Korea). The animals had free access to irradiation-sterilized dry pellet-type feeds and water during the study period. In accordance with the study schedule, the mice were sacrificed by CO_2 inhalation at the end of test substance administration. All animal experimental protocols were reviewed and approved by the Institutional Animal Care and Use Committee board in the Cell Biotech (IACUC, approval No.: study I: CBT-2018-02, study II: CBT-2018-03) based on guidance of the Association for Assessment and Accreditation of Laboratory Animal Care (AAALAC).

CRC xenograft mouse model

A xenograft mouse model for CRC was developed using human-derived DLD-1 cells. DLD-1 cells were inoculated in RPMI1640 (Gibco) medium supplemented with 10% FBS (Gibco) and 0.1 mM NEAA (Gibco). At the exponential growth phase, DLD-1 cells were harvested and counted for tumor inoculation. For tumor development, 2×10^6 DLD-1 tumor cells were suspended in 0.1 ml PBS and used to subcutaneously

inoculate the rear right flank of each mouse. Seven days after tumor inoculation, the animals were weighed and measured for tumor volume and then randomly divided into five groups with seven animals each using a randomized block design for homogeneous group formation when the mean tumor size reached approximately 100–150 mm^3 (5 days). Tumor volumes were measured using the following formula: volume = $(width/2)^2$ × length, where length and width represent the largest and shortest tumor diameters, respectively. Mice were euthanized when tumor volume reached approximately 3000 mm^3. This end-point tumor size was chosen to maximize the number of tumor doublings within the exponential growth phase in the untreated group. Inhibition ratios were determined by IR (%) = (1-T/C) × 100 where T is the mean tumor weight of the test substance and *C is the mean tumor weight of the negative control group.*

AOM/DSS-induced CRC mouse model

For the AOM/DSS-induced CRC model, cohoused age- and sex-matched 6-week-old mice were intraperitoneally injected with AOM (Sigma) with 12.5 mg/kg body weight on the first day of experiment. After 5 days, mice were treated with 2% (wt/vol) DSS (molecular weight 36–50 kDa; MP Biomedicals, Irvine, CA, USA) in their drinking water for 5 days, followed by 16 days of regular water. This cycle was repeated three times.

The presence of occult blood (or gross blood) in the rectum and body weight were determined every 5 days each week for each mouse. Bleeding analysis was scored as 0 when there was no blood in the hemoccult test, 1 for a positive hemoccult result, 2 for slight bleeding, and 3 for gross bleeding and bleeding around the anus. Weight changes during the experiment were calculated as the percent change in weight compared with the baseline measurement. Survival curves were drawn using the Kaplan-Meier method in Prism (version 8.0.2, Graph Pad Software, Inc.). Mice were sacrificed on day 68 and histopathological examination were assessed to measure colon length and number of polyps.

Administration of anticancer drugs

For the CRC xenograft model, mice were randomly divided into different treatment groups when their average body weight reached 22±2 g. Average mean tumor sizes were 100 – 1500 mm^3 (n = 10) 7 days post tumor inoculation. Oral administration started with 0.9% saline (control), 60 mg/kg gemcitabine, $1×10^{10}$ CFU/head PP* and $1×10^{10}$ CFU/head of PP*-P8. The treatment was administered five times each week for 6 weeks. As a positive control, 60 mg/kg gemcitabine were intraperitoneally injected twice a week. For the AOM/DDS induced CRC model, mice were randomly divided into treatment groups (n = 10) when the average body weight reached to 22±2 g. To test anticancer activity of the synthetic probiotics, 0.9% saline (control), $1×10^{10}$ CFU/head PP*, $1×10^{10}$ CFU/head of PP*-P8, and $1×10^{10}$ CFU/head of PP WT were orally administrated to each group five times a week for 68 days. Administration of 60 mg/kg gemcitabine or 40 mg/kg 5-FU were intraperitoneally injected twice a week as positive controls.

Western blot

PP*-P8 on MRS agar plates were used to inoculate 10 ml MRS broth containing 10 μg/ml erythromycin and cultured at 37 ℃ for 15 h without shaking. One milliliter of pre-culture was used to inoculate 10 ml modified M9 medium containing 10 μg/ml erythromycin and cultured at 37 ℃ for 48 h without shaking. Next, 5 ml of the culture was centrifuged, and the supernatant was collected. The supernatant was concentrated using the TCA precipitation method (25% TCA, -20 ℃, 1 h) to isolate total protein. Finally, the P8 protein was detected by western blotting.

To extract total protein from mouse xenograft tissues (DLD-1-derived), the ground tissue powder was lysed in RIPA buffer containing a protease inhibitor cocktail (Roche). Proteins samples were separated by sodium dodecyl sulfate polyacrylamide gel electrophoresis (SDS-PAGE) and transferred to a polyvinylidene difluoride (PVDF) membrane (Amersham Bioscience, Piscataway, NJ, USA). Blotted membranes were blocked in 5% skimmed milk/T-TBS and incubated overnight at 4 °C with the appropriate primary antibodies (rabbit anti-P8 antibody, Young In Frontier Co., Ltd; Seoul, Korea; commercial p53, p21, Cdk1, cyclin B1, and glyceraldehyde 3-phosphate dehydrogenase (GAPDH) antibodies, Cell Signaling Technology, Danvers, MA, USA) diluted 1:1000. The membranes were washed for 15 min three times with TBS-T and then blocked in 5% skimmed milk/TBS-T. The membranes were then incubated for 1 h at 4 ℃ with an HRP-linked secondary antibody (Cell Signaling Technology). GAPDH was used as an internal control. Protein bands were detected using an enhanced chemiluminescence kit (Millipore, Billerica, MA, USA) followed by autoradiography with a Chemi-doc™ Touch Imaging System (Bio-Rad Laboratories, Hercules, CA, USA).

DNA extraction and sequencing

Fecal samples were aseptically collected and frozen at -80 ℃ throughout the experimental period. After the final sampling, all samples were thawed slowly and measured into 200 mg aliquots. DNA was extracted using a Fast DNA SPIN kit for fecal samples (MP Biomedicals, Irvine, CA, USA) according to the manufacturer protocol. Extracted DNA was further processed on an Illumina platform by an external service (Macrogen, Seoul, Korea). The V3-V4 region of the 16S ribosomal RNA gene was targeted for amplicon sequencing using sequence-specific primers (337F: CCTACGGGA(N)GGCWGCAG, 806R: GACTACHVGGGTM(A)TCTAAT) with attached Illumina adapter overhang sequences (Forward: CGTCGGCAGCGTCAGATGTGTATAAGAGACAGCCTACGGGNGGCWGCAG, Reverse: GTCTCGTGGGCTCGGAGATGTGTATAAGAGACAGGACTACHVGGGTATCTAATCC). For library construction, the Herculase II Fusion DNA polymerase Nextera XT index Kit v2 was used and sequenced using the Illumina MiSeq platform.

Bioinformatic analysis of microbial communities

Sequence analysis was performed using QIIME [20] (version 1.9.1). To de-multiplex and trim the forward and reverse fastq files, the split_libraries_fastq.py script was used and reads were filtered with a 25 quality score with 200 bp as a minimum length. Sequences then were clustered into OTUs with a cut-off of 97% identity using the pick_open_reference_otu.py script in QIIME. Taxonomic assignment of OTUs was based on the SILVA 16S rRNA gene database. The Biom file and phylogenetic distances were

imported into R Studio (version 1.1.383, R Studio, Inc., Boston, MA, USA) for further analysis. The OTU table was rarefied by random subsampling without replacement to stimulate even number of reads per sample. To validate the results, sequences were re-analyzed using the QIIME 2 [52] (version 2018.4.)

Alpha diversity including richness (i.e., number of observed OTUs) and Inverse Simpson indices were measured with phyloseq (version 1.30.0) and vegan (version 2.5-6) packages in R. Unweighted uniFrac PCoA was conducted with Bray-Curtis distance and permutational multivariate analysis of variance (PERMANOVA) tests using 999 permutations to evaluate group dissimilarity using the Adonis function in the vegan R package. To determine taxa that had significantly different abundance between control and treatment groups, LEfSe [22] was calculated to find biomarkers with the factorial Kruskal-Wallis test ($P < 0.05$); the logarithmic LDA threshold score was set at 2.0. A correlation matrix was generated using a pairwise spearman rank correlation coefficient between the top 1% abundant taxon and only correlations that had a significant value ($P < 0.05$) defined with corrplot (version 0.84) package were used in further analyses.

Statistical analysis

The animal studies data were statistically analyzed in Prism (version 8.0.2, Graph Pad Software, Inc.) and results are presented as means with standard deviation (mean ± SD). Data from animal studies were evaluated using a one-way or two-way ANOVA followed by Tukey's multiple comparison post-test or Bonferroni's multiple comparison test if significant differences were observed. Unpaired, two-tailed *t*-tests for single comparisons or Wilcoxon rank-sum test were used to assess the significance of the differences in western blot data or bleeding score data. A value of $P < 0.05$ was considered to be statistically significant. A PERMANOVA test with 999 permutations was used to test group dissimilarity using the Adonis function in the vegan R package.

Declarations

Ethics approval and consent to participate

Not applicable.

Consent for publication

Not applicable.

Availability of data and material

The nucleotide sequences used in this study have been deposited in GenBank under the BioProject number PRJNA610226, which comprises 84 Sequence Read Archive files for pyrosequencing reads of the 16S rRNA gene for the fecal microbiotas of AOM/DSS-induced CRC mice.

(https://dataview.ncbi.nlm.nih.gov/object/PRJNA610226?reviewer=noeo8u0bmthnsacov3p7nrq48u)

Competing interests

M.J.C. is the chief executive officer of Cell Biotech, Co., Ltd., and Y.R., B.C.A., Y.-S.Y., O.C., T.Y.K., J.Y.A., and H.J.P. are employees of the company. J.F.K. was the principal investigator for a contract research project of the World Class 300 Project awarded to Cell Biotech. Y.C. worked for Cell Biotech before she became a full-time graduate student at Yonsei University.

Funding

This study was supported by the World Class 300 Project [SMBA, S2367890 (S2416714)], funding from the Small and Medium Business Administration, Korea. Publication was supported in part by the Brain Korea 21 PLUS program, and Y.C. and J.K.Y. are fellowship awardees of this program.

Authors' contributions

M.J.C. and J.F.K. conceived, organized, and supervised the project. J.F.K., Y.C., B.C.A., and M.J.C. interpreted the results and prepared the manuscript. S.-K.K. contributed to experimental design. Cell Biotech, Co. constructed the synthetic probiotic and performed the animal experiments; the JFK lab collected and analyzed the microbiota data. Y.R. and O.C. designed and generated DDS. B.C.A., H.J.P., and J.Y.A. performed *in vitro* assays. Y.-S.Y., T.Y.K., and J.Y.A. were responsible for animal experiments. Y.C. isolated fecal DNA and carried out microbiota and statistical analyses. J.K.Y. contributed to verifying microbiota results. All authors read and approved the final version of the manuscript before submission.

Acknowledgements

We thank the members of Cell Biotech, Co. and the JFK laboratory including Jin-young Lee, and Dowoon Kim, who participated in the project.

Abbreviations

CRC: colorectal cancer; AOM: azoxymethane; DSS: dextran sodium sulfate; LABs: lactic acid bacteria; DDS: drug delivery system; D-Ala: D-alanine; PK: pyruvate kinase; PP-P8: wild-type *P. pentosaceus* SL4 (-7) with the PK-PK promotor system in pCBT24-2; PP*-P8: Δ*alr* mutant with the PK-PK promotor system in the *alr* vector; PP WT: wild-type *P. pentosaceus* SL4; OTUs: operational taxonomical units; PCoA: principal coordinates analysis; LDA: linear discriminant analysis; LEfSe: linear discriminant analysis and effect size; MRS: Man; Rogosa and Sharpe; LB: lysogeny broth; RPMI: Roswell Park Memorial Institute; TBS: Tris-Buffered-Saline Buffer; TBS-T: Tris-Buffered-Saline Buffer with 0.05% Tween 20; PBS: phosphate-buffered saline; PVDF: polyvinylidene difluoride; GAPDH: glyceraldehyde 3-phosphate dehydrogenase; PERMANOVA: permutational multivariate analysis of variance.

References

1. Wang H. Global, regional, and national life expectancy, all-cause mortality, and cause-specific mortality for 249 causes of death, 1980–2015: a systematic analysis for the Global Burden of Disease Study 2015. Lancet. 2016;388:1459–544.
2. Woods D, Turchi JJ. Chemotherapy induced DNA damage response convergence of drugs and pathways. Cancer Biol Ther. 2013;14:379–89.
3. Aggarwal S. Targeted cancer therapies. Nat Rev Drug Discov. 2010;9:427–8.
4. Dolgin E. Microbe fighting with cancer. Nature. 2020;577:16–8.
5. Riglar DT, Silver PA. Engineering bacteria for diagnostic and therapeutic applications. Nat Rev Microbiol. 2018;16:214–25.
6. Zhou S, Gravekamp C, Bermudes D, Liu K. Tumour-targeting bacteria engineered to fight cancer. Nat Rev Cancer. 2018;18:727–43.
7. Górska A, Przystupski D, Niemczura MJ, Kulbacka J. Probiotic bacteria: A promising tool in cancer prevention and therapy. Curr Microbiol. 2019;76:939–49.
8. Zhong L, Zhang X, Covasa M. Emerging roles of lactic acid bacteria in protection against colorectal cancer. World J Gastroenterol. 2014;20:7878–86.
9. Bermúdez-Humarán LG, Langella P. Live bacterial biotherapeutics in the clinic. Nat Biotechnol. 2018;36:816–8.
10. Dekker E, Tanis PJ, Vleugels JLA, Kasi PM, Wallace MB. Colorectal cancer. Lancet. 2019;394:1467–80.
11. An BC, Ryu Y, Yoon Y-S, Choi O, Park HJ, Kim TY, et al. Colorectal cancer therapy using a *Pediococcus pentosaceus* SL4 drug delivery system secreting lactic acid bacteria-derived Protein p8. Mol Cells. 2019;42:755–62.
12. Semjonovs P, Zikmanis P. Evaluation of novel lactose-positive and exopolysaccharide-producing strain of *Pediococcus pentosaceus* for fermented foods. Eur Food Res Technol. 2008;227:851–6.
13. Dantoft SH, Bielak M, Seo J, Chung M, Jensen R. Complete genome sequence of *Pediococcus pentosaceus* Strain SL4. Genome Announc. 2013;1:3–4.
14. Caldwell SL, McMahon DJ, Oberg CJ, Broadbent JR. Development and characterization of lactose-positive *Pediococcus* species for milk fermentation. Appl Environ Microbiol. 1996;62:936–41.
15. Beresford TP, Fitzsimons NA, Brennan NL, Cogan TM. Recent advances in cheese microbiology. Int Dairy J. 2001;11:259–74.
16. Dubey V, Ghosh AR, Bishayee K, Khuda-Bukhsh AR. Probiotic *Pediococcus pentosaceus* strain GS4 alleviates azoxymethane-induced toxicity in mice. Nutr Res. 2015;35:921–9.
17. Ghosh B, Sukumar G, Ghosh AR. Purification and characterization of pediocin from probiotic *Pediococcus pentosaceus* GS4, MTCC 12683. Folia Microbiol. 2019;64:765–78.
18. Thirabunyanon M, Hongwittayakorn P. Potential probiotic lactic acid bacteria of human origin induce antiproliferation of colon cancer cells via synergic actions in adhesion to cancer cells and short-chain fatty acid bioproduction. Appl Biochem Biotechnol. 2013;169:511–25.

19. Ma W, Mao Q, Xia W, Dong G, Yu C, Jiang F. Gut microbiota shapes the efficiency of cancer therapy. Front Microbiol. 2019;10:1050.
20. Caporaso JG, Kuczynski J, Stombaugh J, Bittinger K, Bushman FD, Costello EK, et al. QIIME allows analysis of high- throughput community sequencing data. Nat Methods. 2010;7:335–6.
21. Bray JR, Curtis JT. An ordination of the upland forest communities of Southern Wisconsin. Ecol Monogr. 1957;27:325–49.
22. Segata N, Izard J, Waldron L, Gevers D, Miropolsky L, Garrett WS, et al. Metagenomic biomarker discovery and explanation. Genome Biol. 2011;12:R60.
23. Toso JF, Gill VJ, Hwu P, Marincola FM, Restifo NP, Schwartzentruber DJ, et al. Phase I study of the intravenous administration of attenuated *Salmonella typhimurium* to patients with metastatic melanoma. J Clin Oncol. 2002;20:142–52.
24. Huh WK, Brady WE, Moore KN, Lankes HA, Monk BJ, Aghajanian C, et al. A phase 2 study of live-attenuated *Listeria monocytogenes* cancer immunotherapy (ADXS11-001) in the treatment of persistent or recurrent cancer of the cervix (GOG-0265). J Clin Oncol. 2014;32:TPS5617–7.
25. Staedtke V, Roberts NJ, Bai RY, Zhou S. *Clostridium novyi*-NT in cancer therapy. Genes Dis. 2016;3:144–52.
26. Yang Y, Xia Y, Chen H, Hong L, Feng J, Yang J, et al. The effect of perioperative probiotics treatment for colorectal cancer: Short-term outcomes of a randomized controlled trial. Oncotarget. 2016;7:8432–40.
27. Zhu W, Miyata N, Winter MG, Arenales A, Hughes ER, Spiga L, et al. Editing of the gut microbiota reduces carcinogenesis in mouse models of colitis-associated colorectal cancer. J Exp Med. 2019;216:2378–93.
28. Ho CL, Tan HQ, Chua KJ, Kang A, Lim KH, Ling KL, et al. Engineered commensal microbes for diet-mediated colorectal-cancer chemoprevention. Nat Biomed Eng. 2018;2:27–37.
29. Chowdhury S, Castro S, Coker C, Hinchliffe TE, Arpaia N, Danino T. Programmable bacteria induce durable tumor regression and systemic antitumor immunity. Nat Med. 2019;25:1057–63.
30. An BC, Hong S, Park HJ, Kim BK, Ahn JY, Ryu Y, et al. Anti-colorectal cancer effects of probiotic-derived P8 Protein. Genes (Basel). 2019;10.
31. Guthrie L, Gupta S, Daily J, Kelly L. Human microbiome signatures of differential colorectal cancer drug metabolism. npj Biofilms Microbiomes. 2017;3:27.
32. Praveschotinunt P, Duraj-Thatte AM, Gelfat I, Bahl F, Chou DB, Joshi NS. Engineered *E. coli* Nissle 1917 for the delivery of matrix-tethered therapeutic domains to the gut. Nat Commun. 2019;10:5580.
33. MY Z. Mechanisms of inflammation-driven bacterial dysbiosis in the gut. Mucosal Immunol. 2016;10:18–26.
34. Routy B, Gopalakrishnan V, Daillère R, Zitvogel L, Wargo JA, Kroemer G. The gut microbiota influences anticancer immunosurveillance and general health. Nat Rev Clin Oncol. 2018;15:382–96.

35. Jiang SM, Wu JH, Jia L. Intervention of Mirtazapine on gemcitabine-induced mild cachexia in nude mice with pancreatic carcinoma xenografts. World J Gastroenterol. 2012;18:2867–71.
36. Aston WJ, Hope DE, Nowak AK, Robinson BW, Lake RA, Lesterhuis WJ. A systematic investigation of the maximum tolerated dose of cytotoxic chemotherapy with and without supportive care in mice. BMC Cancer. 2017;17:684.
37. Rübe CE, Wilfert F, Uthe D, König J, Liu L, Schuck A, et al. Increased expression of pro-inflammatory cytokines as a cause of lung toxicity after combined treatment with gemcitabine and thoracic irradiation. Radiother Oncol. 2004;72:231–41.
38. Schneeberger M, Everard A, Gómez-Valadés AG, Matamoros S, Ramírez S, Delzenne NM, et al. *Akkermansia muciniphila* inversely correlates with the onset of inflammation, altered adipose tissue metabolism and metabolic disorders during obesity in mice. Sci Rep. 2015;5:16643.
39. Dao MC, Everard A, Aron-Wisnewsky J, Sokolovska N, Prifti E, Verger EO, et al. *Akkermansia muciniphila* and improved metabolic health during a dietary intervention in obesity: Relationship with gut microbiome richness and ecology. Gut. 2016;65:426–36.
40. Cani PD, de Vos WM. Next-generation beneficial microbes: The case of *Akkermansia muciniphila*. Front Microbiol. 2017;8:1765.
41. Bosshard PP, Zbinden R, Altwegg M. *Turicibacter sanguinis* gen. nov., sp. nov., a novel anaerobic, Gram-positive bacterium. Int J Syst Evol Microbiol. 2002;52:1263–6.
42. O'Cuív P, Klaassens ES, Durkin AS, Harkins DM, Foster L, McCorrison J, et al. Draft genome sequence of *Turicibacter sanguinis* PC909, isolated from human feces. J Bacteriol. 2011;193:1288–9.
43. Kellermayer R, Dowd SE, Harris RA, Balasa A, Schaible TD, Wolcott RD, et al. Colonic mucosal DNA methylation, immune response, and microbiome patterns in Toll-like receptor 2-knockout mice. FASEB J. 2011;25:1449–60.
44. Rausch P, Steck N, Suwandi A, Seidel JA, Künzel S, Bhullar K, et al. Expression of the bood-goup-related gene B4galnt2 alters susceptibility to *Salmonella* Infection. PLoS Pathog. 2015;11:e1005008.
45. Dimitriu PA, Boyce G, Samarakoon A, Hartmann M, Johnson P, Mohn WW. Temporal stability of the mouse gut microbiota in relation to innate and adaptive immunity. Environ Microbiol Rep. 2013;5:200–10.
46. Longley DB, Harkin DP, Johnston PG. 5-Fluorouracil: Mechanisms of action and clinical strategies. Nat Rev Cancer. 2003;3:330–8.
47. Bracht K, Nicholls AM, Liu Y, Bodmer WF. 5-Fluorouracil response in a large panel of colorectal cancer cell lines is associated with mismatch repair deficiency. Br J Cancer. 2010;103:340–6.
48. Patel K, Anthoney DA, Crellin AM, Sebag-Montefiore D, Messruther J, Seymour MT. Weekly 5-fluorouracil and leucovorin: Achieving lower toxicity with higher dose-intensity in adjuvant chemotherapy after colorectal cancer resection. Ann Oncol. 2004;15:568–73.
49. Touil Y, Igoudjil W, Corvaisier M, Dessein AF, Vandomme J, Monte D, et al. Colon cancer cells escape 5FU chemotherapy-induced cell death by entering stemness and quiescence associated with the c-Yes/YAP axis. Clin Cancer Res. 2014;20:837–46.

50. Boige V, Mendiboure J, Pignon JP, Loriot MA, Castaing M, Barrois M, et al. Pharmacogenetic assessment of toxicity and outcome in patients with metastatic colorectal cancer treated with LV5FU2, FOLFOX, and FOLFIRI: FFCD 2000-05. J Clin Oncol. 2010;28:2556–64.
51. Lütke-Eversloh T, Stephanopoulos G. L-Tyrosine production by deregulated strains of *Escherichia coli*. Appl Microbiol Biotechnol. 2007;75:103–10.
52. Bolyen E. Reproducible, interactive, scalable and extensible microbiome data science using QIIME 2. Nat Biotechnol. 2019;37:848–57.

Figures

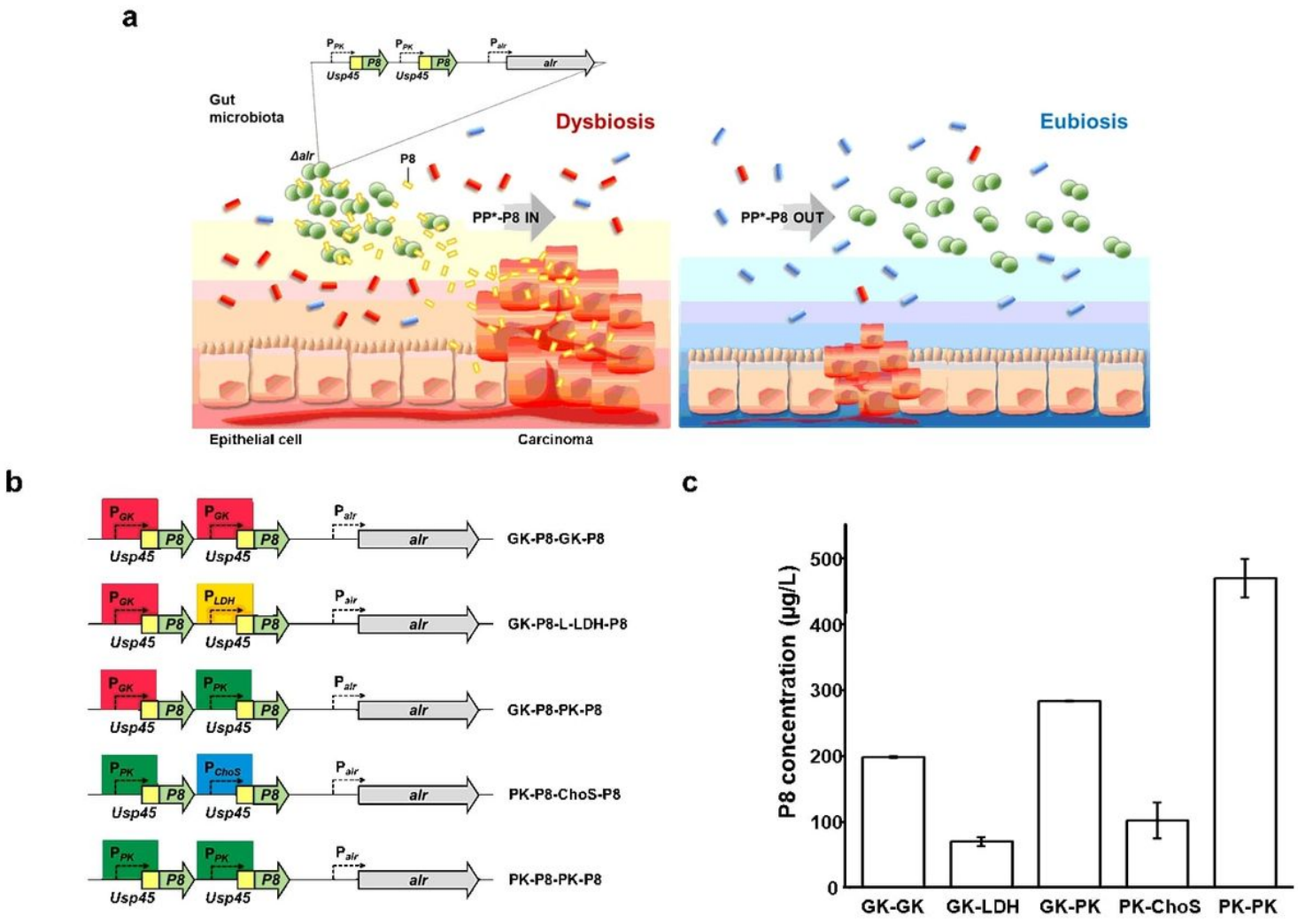

Figure 1

Module design of a lactic acid bacterium-based drug delivery system for optimal P8 productivity. a A schematic outline depicting the expected mode of action of the synthetic probiotic PP*-P8 with the alr complementation system. alr, the alanine racemase gene. b Constructs with various promoters for dual expression of the P8 therapeutic protein fused to the 27-residue Usp45 leader peptide. GK, glucose kinase; LDH, L-lactate dehydrogenase; PK, pyruvate kinase; ChoS, choline ABC transporter permease and

substrate binding protein. c Concentrations of P8 secreted from PP*-P8 that were quantified using ELISA, indicating that the PK-PK promotor system had the highest amount of secreted P8.

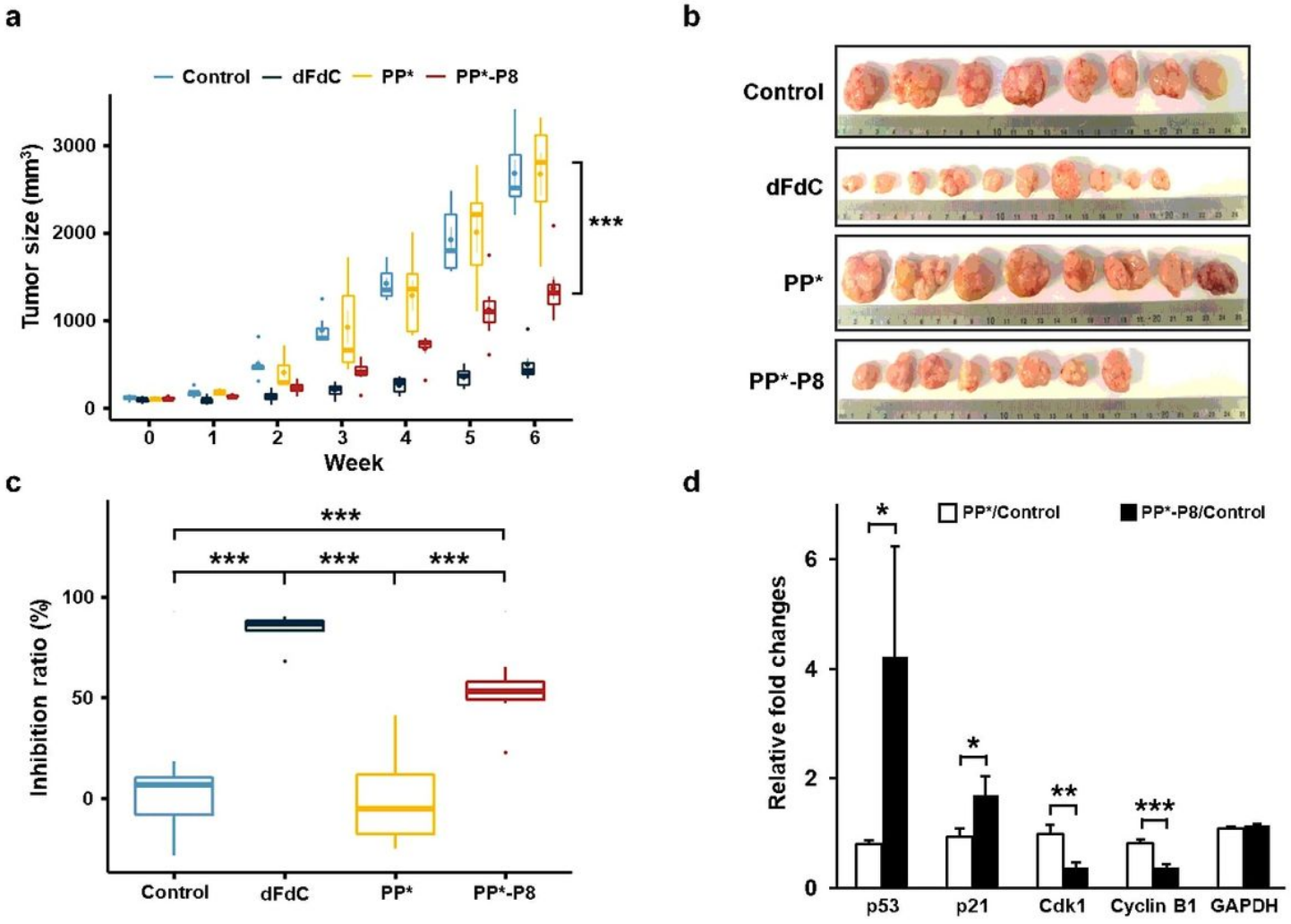

Figure 2

Anti-tumor efficacy of the PP*-P8 probiotic in the DLD-1 xenograft mouse model. a Increased sizes of DLD-1-derived tumors recorded each week. Mice (n = 10 in each group) were subcutaneously inoculated with 2×10^6 DLD-1 cells in the rear right flank and then received 0.9% saline (control), 60 mg/kg body weight gemcitabine (dFdC; intraperitoneal injection, twice a week), 1×10^10 CFU/head P. pentosaceus alr (pCBT24-2-alr) (PP*; oral administration, five times a week), or 1×1010 CFU/head P. pentosaceus alr (pCBT24-2-PK-p8-PK-p8-alr) (PP*-P8; oral administration, five times a week). ***P < 0.001 for control vs. dFdC, control vs. PP*-P8, dFdC vs. PP*, PP* vs. PP*-P8. b Extracted tumor tissues from each treatment group 6 weeks after the DLD-1 xenograft. c Inhibition ratios for tumor growth calculated from the mean tumor weights of the control group and the test groups. ***P < 0.001. d Relative fold changes in the expression of cell cycle regulatory factors between PP* with control and PP*-P8 with control. Each vertical bar represents the arithmetic mean of three replicates. *P < 0.05, **P < 0.01, ***P < 0.001.

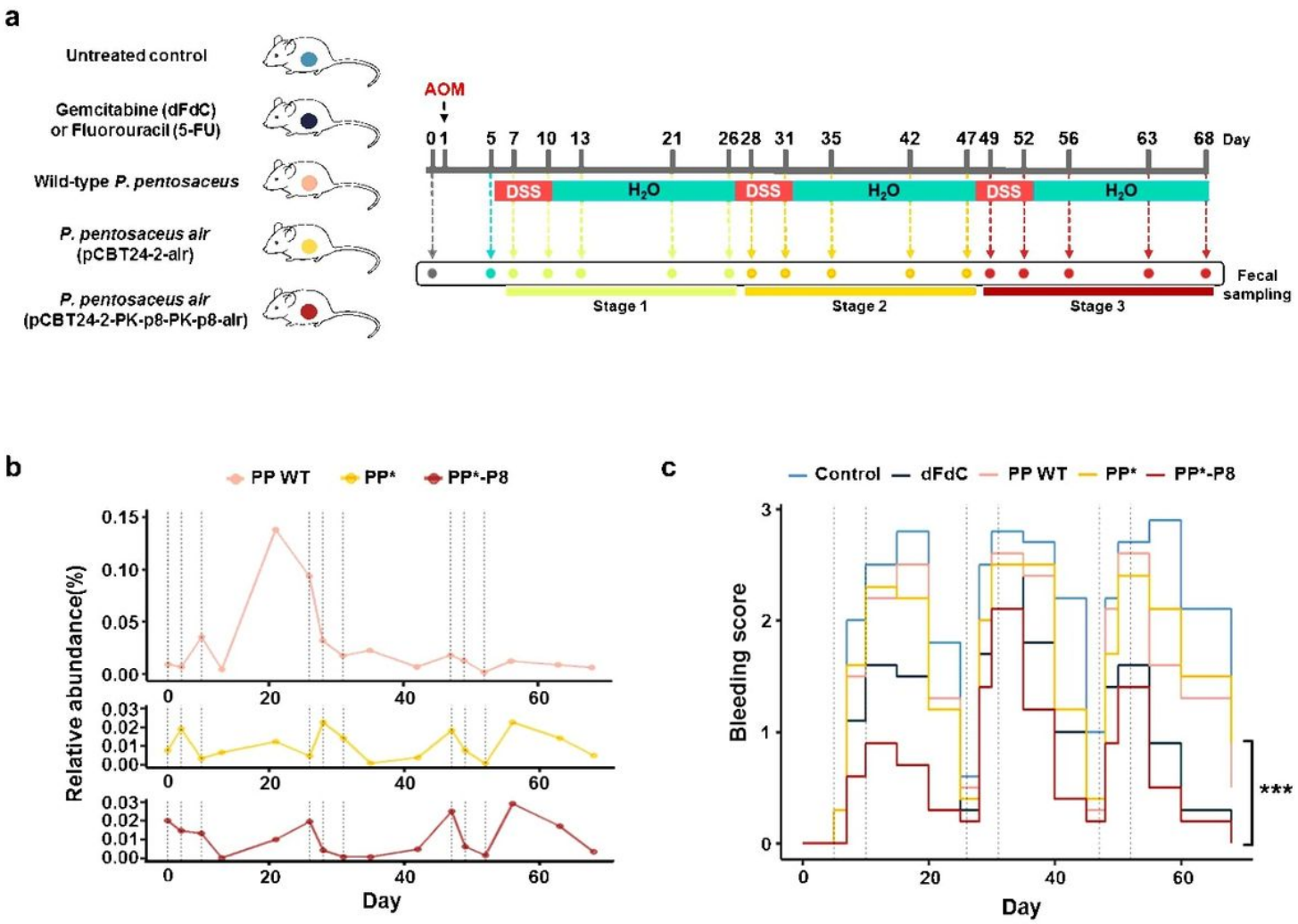

Figure 3

AOM/DSS-induced mouse model of colitis-associated colon carcinogenesis. a The experimental scheme for tumor induction by azoxymethane (AOM) and dextran sodium sulfate (DSS). Mice (n = 10 in each group) were intraperitoneally injected with 12.5 mg/kg body weight AOM on day 1 and on day 5, they were given water containing 2% w/v DSS for 5 days, followed regular water for 16 days, which was repeated three times during the 68-day treatment. Treatment groups: untreated control (0.9% saline, oral), gemcitabine (dFdC; 60 mg/kg body weight, intraperitoneal, twice a week) or fluorouracil (5-FU; 40 mg/kg body weight, intraperitoneal, twice a week), wild type P. pentosaceus (PP WT; 1×1010 CFU/head, oral, five times a week), P. pentosaceus alr (pCBT24-2-alr) (PP*; 1×10^10 CFU/head, oral, five times a week), and P. pentosaceus alr (pCBT24-2-PK-p8-PK-p8-alr) (PP*-P8; 1×1010 CFU/head, oral, five times a week). Schedule for fecal sampling are indicated with arrows. b Temporal dynamics of the PP*-P8 population in relative abundance during the experimental period. Dashed lines represent the DSS treatment episodes. c Bleeding scores were assessed every 5 days by hemoccult testing and visible signs. ***P < 0.001 for control vs. dFdC, control vs. PP*-P8, PP* vs. dFdC, PP* vs. PP*-P8.

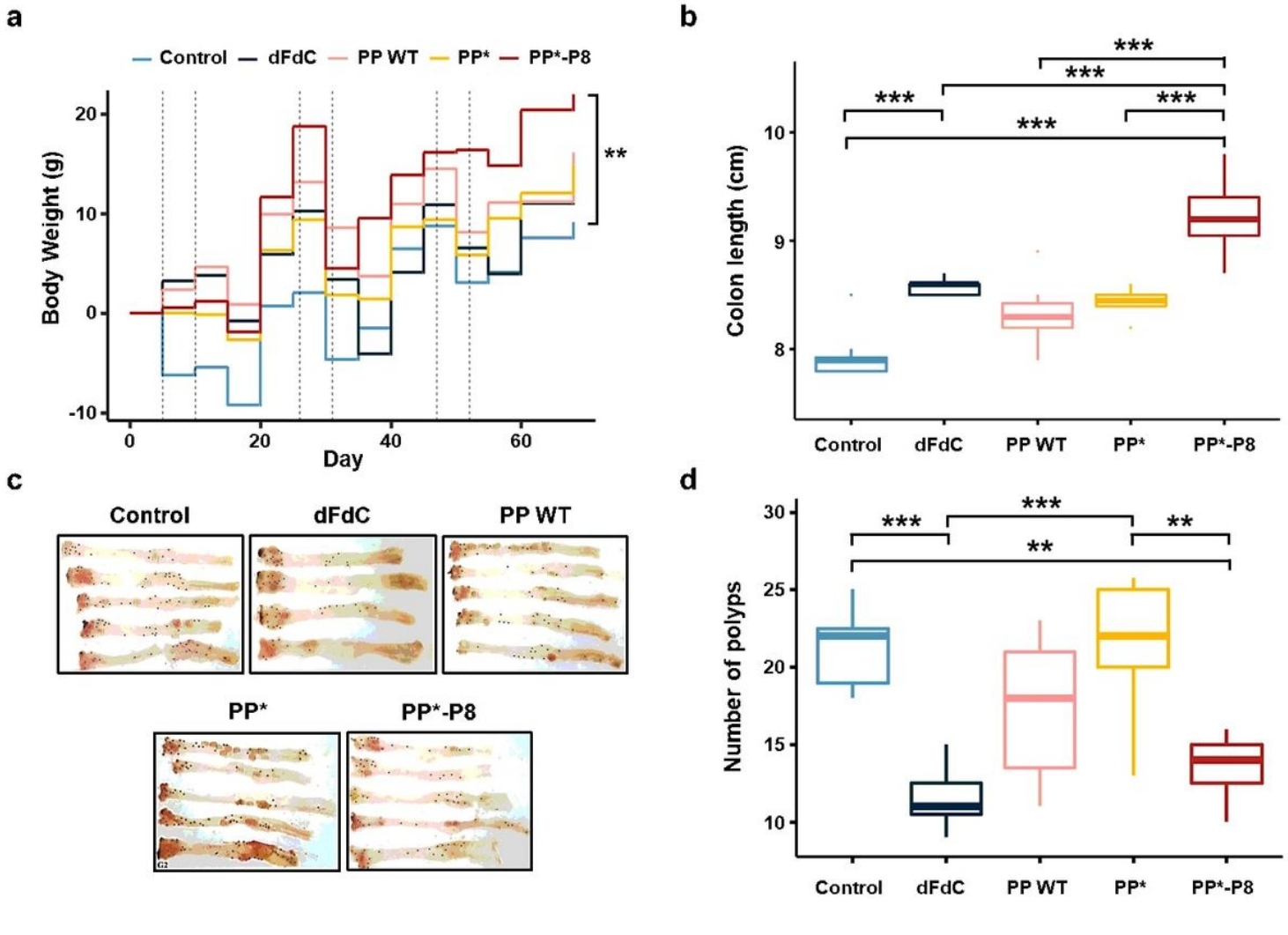

Figure 4

Effects of PP*-P8 on general health and tumorigenesis in the AOM/DSS mouse model. a Changes in the body weight of mice were recorded each week. Treatments: dFdC, gemcitabine; PP WT, wild type P. pentosaceus; PP*, P. pentosaceus alr (pCBT24-2-alr); PP*-P8, P. pentosaceus alr (pCBT24-2-PK-p8-PK-p8-alr). **P < 0.01. b Colon length was measured after 68 days. ***P < 0.001. c Macroscopic and histopathological appearance of polyps and carcinomas. d Number of adenocarcinomas. ***P < 0.001.

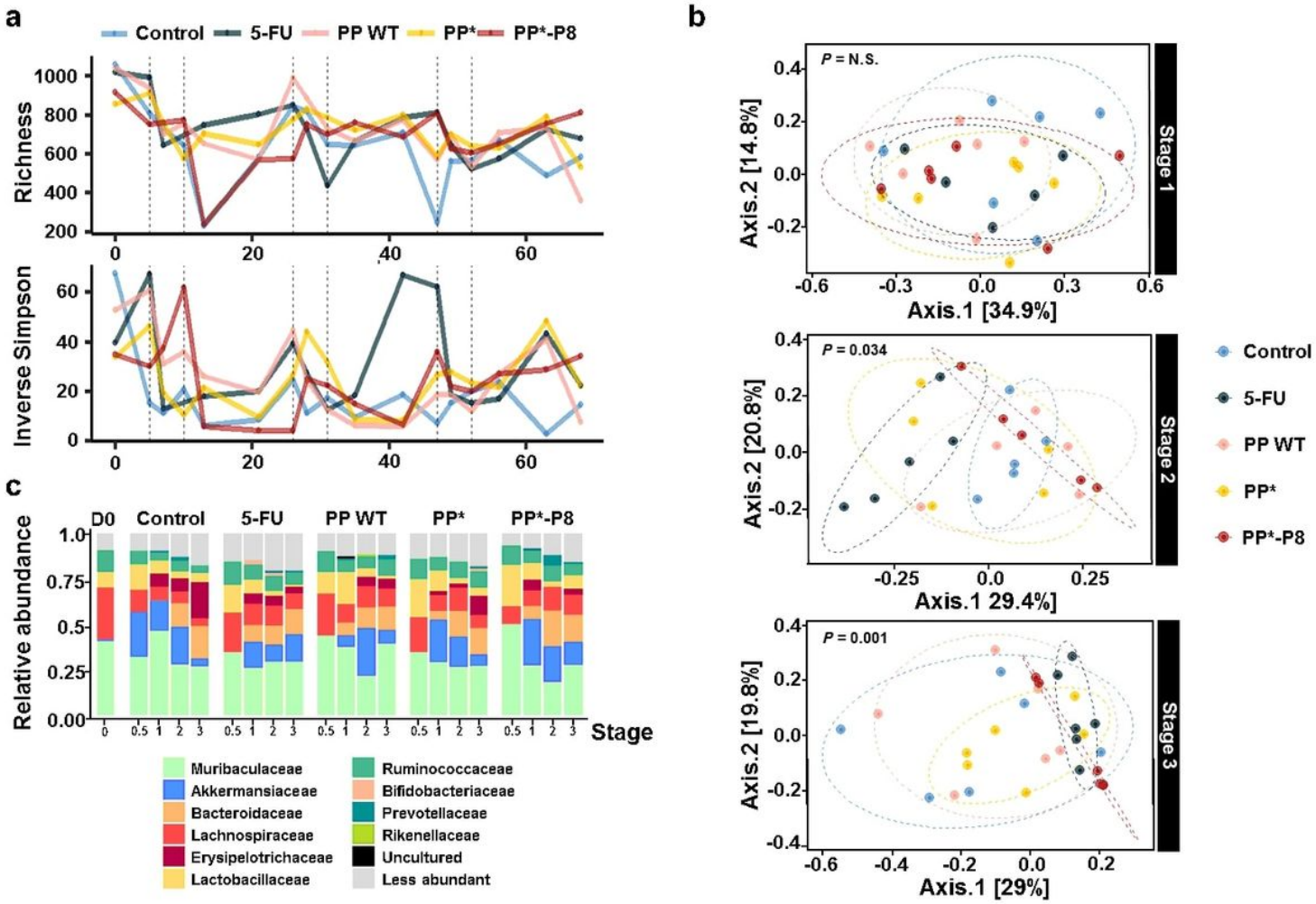

Figure 5

Longitudinal analyses of the gut microbiota of AOM/DSS mice treated with PP*-P8 a Changes in alpha diversity indices of microbial communities in the fecal samples. Species richness is plotted as the number of operational taxonomic units and the inverse Simpson index. Treatments: 5-FU, fluorouracil; PP WT, wild type P. pentosaceus; PP*, P. pentosaceus alr (pCBT24-2-alr); PP*-P8, P. pentosaceus alr (pCBT24-2-PK-p8-PK-p8-alr). b Principal coordinate analysis based on Bray-Curtis dissimilarity. Each dot indicates a single sample and each group is shown in a different color. P-values correspond to the permutational multivariate analysis of variance results. c Microbial composition at the family level is shown as relative abundance. Except for stage 0.5, which shows a single sample, proportions are the averages of five samples. D0, day 0.

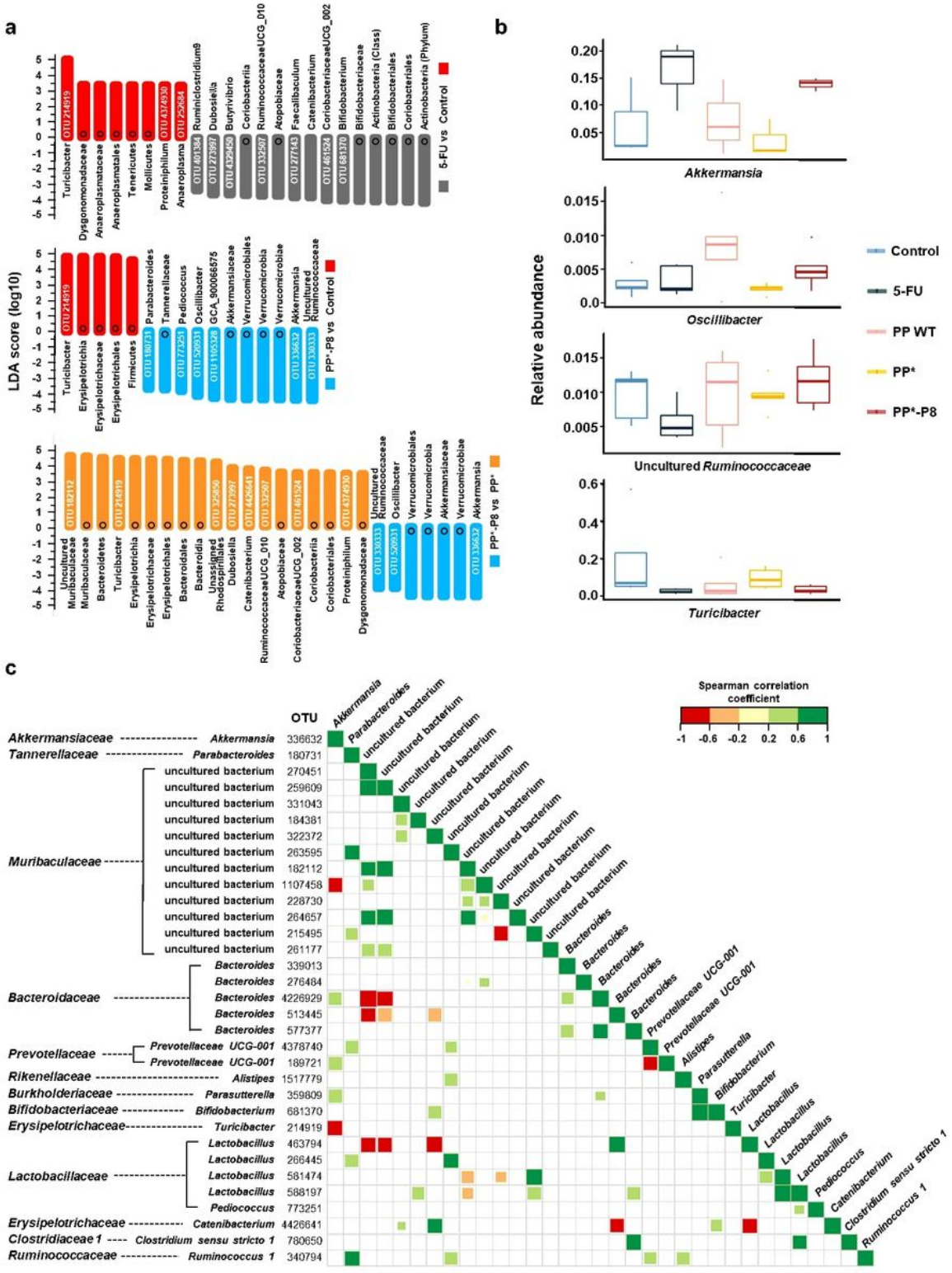

Figure 6

Specific microbial taxa likely associated with differences between the treatment groups. a Linear discriminant analysis effect size of samples after the final DSS administration. 5-FU, fluorouracil; PP*, P. pentosaceus alr (pCBT24-2-alr); PP*-P8, P. pentosaceus alr (pCBT24-2-PK-p8-PK-p8-alr). Black circles represent multiple sibling taxa. b Relative abundance of four selected operational taxonomic units, Akkermansia, an uncultured Ruminococcaceae, Oscillibacter, and Turicibacter in stage 3. c Positive and

negative correlation matrix between the top 1% abundant bacterial taxa. Results of a pairwise Spearman's rank correlation coefficients after the final DSS administration are shown. Correlations with $P < 0.05$ were visualized using the corrplot package. Green, positive correlation; red, negative correlation. Square size symbolizes the measure of the correlation coefficient.

Supplementary Files

This is a list of supplementary files associated with this preprint. Click to download.

- Additionalfile208082020MicrobiomeS.pdf
- Additionalfile108082020Microbiome.docx